Received 10 November 2023; accepted 4 December 2023. Date of publication 8 December 2023; date of current version 30 January 2024.

Digital Object Identifier 10.1109/OJAP.2023.3340896

The Path Reduction Factor for the Prediction of Rain Attenuation Affecting Short EHF Terrestrial Links

FRANCESCO CAPELLETTI[1], CARLO RIVA[1] (Senior Member, IEEE), GIUSEPPE ROVEDA[2], AND LORENZO LUINI[1] (Senior Member, IEEE)

[1]Dipartimento di Elettronica, Informazione e Bioingegneria, Politecnico di Milano, 20133 Milan, Italy
[2]R&D Department, Huawei Technologies S.r.l., 20147 Milan, Italy

CORRESPONDING AUTHOR: L. LUINI (e-mail: lorenzo.luini@polimi.it)

ABSTRACT The path reduction factor (PRF), a key element of semi-empirical rain attenuation statistics prediction models, is investigated to shed some light on its value for links shorter than 1 km. PRF is here calculated from simulations underpinned by the use of the Enhanced Synthetic Storm Technique (E-SST) to take into account the rain rate spatial distribution along the path. This novel approach, in contrast with the more customary one of inferring a PRF model from measurements, offers the advantage of avoiding considering any unwanted additional attenuation not due to precipitation, but typically linked to system-induced effects. Results indicate that, as expected, PRF reduces with the increase in the rain rate R and in the path length L, and they also reveal quite a marginal dependence on the operational frequency. Most importantly, the outcomes highlight that the maximum values of PRF only slightly exceeds 1 and, in addition, they provide a possible explanation as to why, on the contrary, the path reduction factor defined in the Recommendation ITU-R P.530-18 is characterized by a steep increase as L reduces.

INDEX TERMS 6G mobile networks, atmospheric effects, millimeter waves, radio propagation models, terrestrial links.

I. INTRODUCTION

DATA exchange via telecommunication systems has been constantly growing worldwide, not only due to the gradual but incessant proliferation of devices connected to the Internet, but also owing to the increasingly advanced multimedia and broadcast services offered to users [1]. Data rates in the order of hundreds of megabits per single user call for the availability of large bandwidths, which can be supported by high carrier frequencies. This is definitely the case for the fifth-generation of mobile communication systems (5G), which makes use of frequencies up to 26-28 GHz for the access link [2], and of millimeter waves (currently E band, but D band and beyond in the near future) for the backhaul links aggregating the high data rate traffic of multiple users.

Unfortunately, the increase in the carrier frequency is associated to the correspondent enhancement of the detrimental effects significantly impairing the propagation of electromagnetic waves in the troposphere. Among them, rain attenuation definitely plays the most relevant role in reducing the channel quality, at any frequency between 10 GHz and 1 THz: the transmitted signal is dissipated, scattered, and depolarized by rain drops [3].

As the impact of precipitation increases, so does the importance of using accurate models aimed at predicting rain attenuation for terrestrial links, which, in turn, is key for system design purposes [4]. A class of the currently available models relies on the realistic representation of the spatial distribution of the rain intensity: while such prediction methods typically offer a good global accuracy, they are also more complex and computationally intensive. This is the case, for example, of the EXCELL (EXponential CELL) [5] and MultiEXCELL [6] models, which define a population of circularly symmetrical, exponentially-profiled rain cells to reproduce the rainfall environment affecting the link starting from the point rain rate statistical distribution [4], [7], [8]. On the other hand, alternative semi-empirical statistical approaches have been developed in the past to offer simpler yet effective prediction models. The common element to all such models is the definition of an empirical component,

typically referred to as Path Reduction Factor (PRF) and discussed in more detail in Section II, that is intended to take into account, in an equivalent manner, the spatial distribution of the rain rate along the link [9]. Indeed, thanks to the introduction of PRF, the calculation of the path rain attenuation is greatly simplified: the knowledge of the rain rate along the whole link is not required, as just its value at the transmitter/receiver side is actually sufficient [10].

PRF included in earlier semi-empirical models was derived from concurrent rain attenuation/rain rate measurements collected in the framework of experimental activities typically involving long paths (e.g., 10 km) [11], [12], [13], [14]. From such works, quite a general consensus emerges on: the decrease in PRF as the path length L becomes longer and the rain rate R more intense [14]; the marginal dependence of PRF on the frequency f. Moreover, the maximum statistical value of PRF was generally found to be limited to 1 [11], or slightly higher than 1 [14].

More recently, PRF has been investigated also for path lengths shorter than 1 km, due to the increasing interest in high-frequency backhaul links for 5G/6G systems [2]. These works show a lower degree of agreement on the results: while some findings seem to indicate that PRF tends to 1 as L decreases [15], some others hint at a steep increase of PRF much beyond such value [16], [17]. The latter have recently (September 2021) prompted to remove the limitation of PRF to 2.5 in the model included in Section III-D of the Recommendation ITU-R P.530 for the prediction of rain attenuation affecting terrestrial links.

This contribution aims at shedding some light on the value of PRF for links shorter than 1 km, specifically it corroborates the assumption that the PRF value converges to 1 as L becomes shorter [10], [11], [13]. To this aim, differently from the works published so far that prevalently rely on measurements to infer analytical functions describing the trend of PRF with R and L [10], [11], [12], in this contribution, PRF is calculated from simulations underpinned by the use of the Enhanced Synthetic Storm Technique (E-SST) to realistically reproduce the rain rate spatial distribution [18].

The paper is structured as follows. Section II recalls the definition of PRF and discusses in more detail the contrasting findings on PRF for short links as derived from measurements. Section III introduces the dataset and the model (E-SST) employed to derive additional results on PRF for short links; this Section also provides a possible explanation as to why PRF was found to increase with the reduction in the path length when using measurements. Finally, Section IV draws some conclusions.

II. PATH REDUCTION FACTOR: DEFINITION AND ISSUES

The rain attenuation affecting a terrestrial link is calculated as:

$$A = \int_L \gamma_R(l)dl \ \text{(dB)} \tag{1}$$

where L is the path length (km) and $\gamma_R(l)$ is the specific attenuation due to rain (dB/km) at position l along the link. γ_R depends on the macro-physical properties (rain rate) and micro-physical ones (e.g., drop water temperature, drop size distribution, drop shape, drop orientation, ...) of precipitation, as well as on the geometrical and electrical features of the link, namely elevation θ, wave frequency f and wave polarization p. From the practical point of view, the specific attenuation due to rain is commonly calculated as:

$$\gamma_R(l) = kR(l)^\alpha \ \text{(dB/km)} \tag{2}$$

where k and α are coefficients tabulated in the Recommendation ITU-R P.838-3 as a function of θ, f and p [19].

It is obvious from (1) that the accurate calculation of A requires full knowledge of the rain intensity along the whole path, which is hardly possible. As an alternative, rain attenuation can be also calculated as:

$$A = \gamma_R(0)\ L_E = k\ R(0)^\alpha\ L\ \ PRF\ \text{(dB)} \tag{3}$$

where L_E is the effective path length.

Equation (3) offers a simplified option for the calculation of the rain attenuation, as it depends just on the rain intensity measured at one side of the link (specifically, the transmitter side, given that $l = 0$ km), the path length and the path reduction factor PRF. The latter is necessarily introduced to take into account that R is not constant along the path: as discussed for example in [5], [6], [7], [20], the spatial distribution of the rain rate can be quite accurately modeled by rain cells characterized by an intense R peak, surrounded by much lower values. As a result, the value of PRF will change depending on the rain cell affecting the link, the path length and the relative position between the cell and the link itself. While it is difficult to predict in advance every single value of PRF, one preliminary consideration can be for sure put forth: PRF is expected to asymptotically reach 1 as $L \to 0$ km. In fact, the change in the rain rate along the link will be more and more limited as the path length decreases, eventually leading to a constant value of R along the whole link. In this case, equation (1) will simply reduce to:

$$A = \int_L \gamma_R(l)dl = kR(0)^\alpha\ L\ \text{(dB)} \tag{4}$$

Comparing (3) and (4) obviously leads to PRF = 1. The outcome of this reasoning is de facto in contrast with the PRF defined in some models available in the literature, such as the rain attenuation prediction method included in the Recommendation ITU-R P.530-18 [21] and the one presented in [16], hereinafter referred to as Budalal model. Concerning the former, PRF was adjusted based on the concurrent rain rate/rain attenuation measurements included in the ITU-R Study Group 3 experimental database (DBSG3): out of 89 entries, 11 are relative to path lengths shorter than 1 km (0.47 km $\leq L \leq$ 0.67 km) and are associated to frequencies covering the 37-137 GHz range.

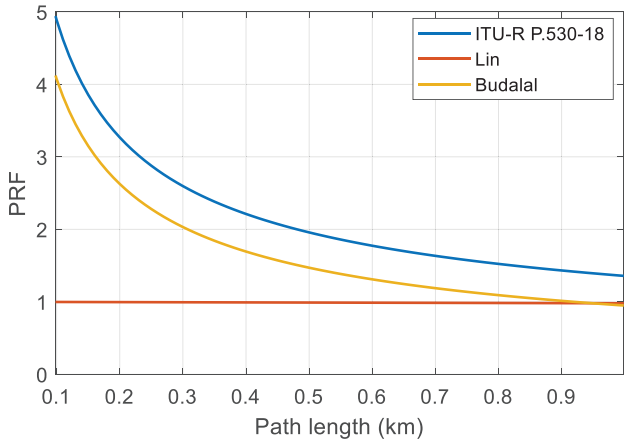

FIGURE 1. Trend of PRF as a function of the path length for different models ($R = 40$ mm/h, $f = 80$ GHz).

Based on these measurements, the following path reduction factor was derived [21]:

$$PRF_{ITU} = \frac{1}{0.477L^{0.633}R^{0.073\alpha}f^{0.123} - 10.579\left(1 - e^{-0.024L}\right)} \tag{5}$$

Figure 1 shows the trend of the ITU-R model PRF as a function of L. Though it is clear from (5) that PRF also depends on the rain rate and the frequency (in Figure 1, $R = 40$ mm/h and $f = 80$ GHz), it can be easily verified that their effect on PRF is quite marginal for such short links. This is not the case for L, whose decrease is associated to a steep increase in PRF much beyond 1.

Figure 1 also includes the trend of PRF as defined in the Budalal model [16], which was determined from the measurements collected by means of two 300-m long terrestrial links operating at 26 and 38 GHz, as well as from additional data available in the literature at frequencies beyond 40 GHz: PRF turns out to increase as L decreases, with a profile very similar to the one of the ITU-R model; its analytical formulation is given by:

$$PRF_B = \begin{cases} \frac{1}{1.77L^{0.77}R^{-0.05}} & \text{for } f \leq 40 \text{ GHz} \\ \frac{1}{0.47L^{0.633}R^{0.073}f^{0.123}} & \text{for } f > 40 \text{ GHz} \end{cases} \tag{6}$$

As a term of reference, Figure 1 also depicts PRF of the Lin model, whose upper limit is 1 when $L = 0$ km, defined as [11]:

$$PRF_L = \frac{2636}{2636 + L(R - 6.2)} \tag{7}$$

A very similar trend characterizes PRF of several other models (not reported here for the sake of brevity), such as [13] and [14].

As a matter of fact, the above discussion highlights contrasting results and conclusions on PRF for links shorter than 1 km, though all derived from experimental data. With the aim of providing additional elements to this debate, Section III presents an alternative approach to derive PRF.

TABLE 1. Main features of the experimental E-band and D-band terrestrial links installed at Politecnico di Milano main campus.

	E-Band	D-Band
Channel bandwidth	250 MHz	
Transmitter power	+10 dBm	+5 dBm
Receiver sensitivity (with QPSK)	-71 dBm	-67 dBm
Antenna gain (both TX and RX)	40 dBi	34 dBi
Wave polarization	Linear vertical	
Carrier frequency	83 GHz	156 GHz
Atmospheric fade margin	36 dB	15 dB
Sample frequency	20 samples/s	5 samples/s

III. PATH REDUCTION FACTOR: A SIMULATION APPROACH

As an alternative to using measurements, PRF can also be calculated by resorting to models, specifically to the Enhanced Synthetic Storm Technique (E-SST), which aims at synthesizing time series of the rain attenuation A from measured rain rate data [18]: to the authors' knowledge, no prior work has yet proposed such an approach to investigate PRF. This methodology for the calculation of PRF is duly detailed in this Section, after a discussion on the experimental data. Specifically, this Section is organized as follows: Section III-A presents the measurements collected using two terrestrial links operating at E band and D band, which are used to assess the accuracy of E-SST in estimating rain attenuation data; Sections III-B and III-C describe the disdrometric data and the wind velocity data, respectively, both of which are used as inputs to E-SST; Section III-D presents a methodology to obtain more accurate estimates of the rain intensity from disdrometric data; Section III-E describes in detail the application of E-SST, which is applied in Sections III-F and III-G to calculate and investigate PRF.

A. TERRESTRIAL LINK DATA

With the aim of assessing the rain attenuation prediction performance of the E-SST for short terrestrial links operating at EHF and thus of corroborating its use to estimate PRF, rain attenuation data extracted from a long-term experimental campaign (from February 2018 to January 2022) are used as a reference in this work. This campaign was conducted using two collocated terrestrial links (path length $L = 325$ m), operating at 83 GHz and 156 GHz, installed between Building 14 and 20 in the main campus of the Politecnico di Milano, in the framework of a collaboration with the Huawei European Microwave Centre in Milan [15], [22]. The main system parameters are summarized in Table 1, which shows that the two links operate with QPSK modulation to maximize the signal-to-noise ratio, i.e., the margin available to measure and characterize tropospheric effects.

The received signal level (RSL) collected at the receiver side, P_{RX}, is accurately time-stamped (synchronized with the coordinated universal time - UTC) and signal spikes

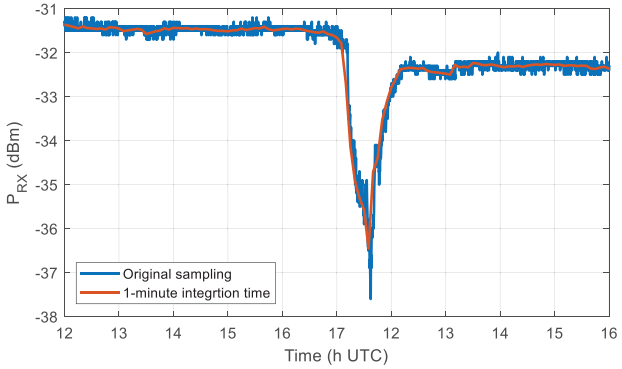

FIGURE 2. E-band data collected on May 13, 2018: original and 1-minute average received power.

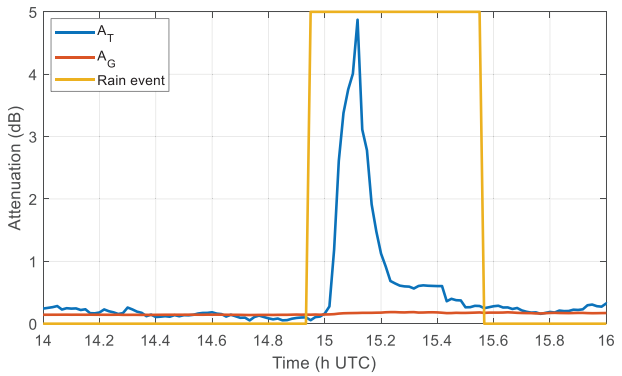

FIGURE 3. Processed data collected on May 13, 2018: total attenuation A_T (blue solid line), reference attenuation due to gases A_G (red solid line) and identified rain event (yellow solid line).

are filtered out by careful visual inspection. Afterward, data are averaged over 1-minute in order to achieve the same integration time of the disdrometer (see Section III-B), as well as to filter out the fast oscillations due to scintillations (see Figure 2).

After pre-processing, data are elaborated to derive the total tropospheric attenuation A_T (i.e., due to gases and rain) from the RSL. This task can in principle be achieved by inverting the link budget equation; in practice, this is hardly possible due to system-induced effects (e.g., change in the antenna pointing due to strong winds, variation in the transmitted power, wet antenna effect, ...), which may alter the actual value of A_T. As described in detail in [15] and [22] for E-band and D-band data, respectively, a more accurate way of extracting A_T from the received power P_{RX} (hence the rain attenuation A_R) is to consider that, in rain-free conditions, A_T coincides with the attenuation induced by gases A_G, which can be accurately estimated using the model included in the Recommendation ITU-R 676-13 (Annex 1) [23]. Conversely, in rainy conditions, starting from A_G and based on the identification of rain events by means of the collocated rain sensors, the isolation of the rain attenuation from A_T is achieved by removing A_G. As an example, Figure 3 reports the processed data collected on May 13, 2018. Using the gaseous attenuation A_G as reference, the difference in P_{RX} before (≈ -31.5 dBm) and after (≈ -32.3 dBm) the rain

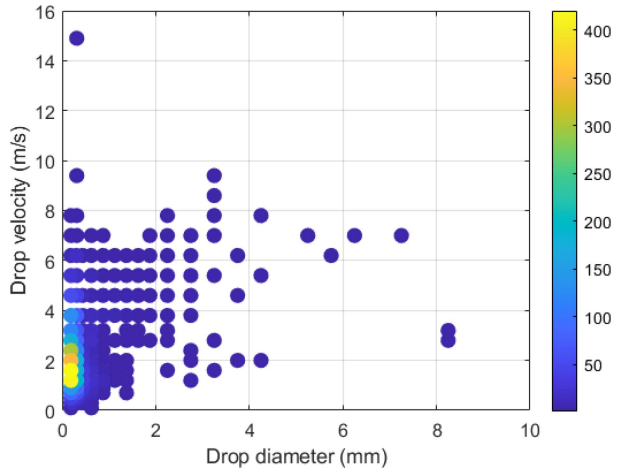

FIGURE 4. Sample 1-minute spectrum collected by the LPM during a rain event occurred on April 4, 2015, 17:07 UTC. The estimated rain rate is 34.91 mm/h.

event in Figure 2 is no longer visible on A_T in Figure 3: this system-induced effect, likely due to a temperature related change in the transmitter/receiver chain and/or to the wet antenna, is thus mitigated for a more accurate extraction of the rain attenuation, which is calculated as $A_R = A_T - A_G$ during the rain event and as $A_R = 0$ dB otherwise.

More information on the experimental setup and on the approach to extract rain attenuation from the received power is provided in [15] and [22], to which the reader is addressed for more details. It is worth underlining that such references also describe the method used to remove the additional attenuation induce by the so called wet antenna effect [24].

B. DISDROMETRIC DATA

The main input to the E-SST are rain rate time series, which, in this work, are collected by the Thies Clima Laser Precipitation Monitor (LPM) installed on the rooftop of Building 20 in the main university campus of Politecnico di Milano. The LPM classifies falling particles, including rain drops, in bidimensional bins identified by diameter and terminal velocity, from which the Drop Size Distribution (DSD) and the rain rate R can be obtained (see Section III-D for more details). The LPM classifies the observed particles into a total of $N_D = 22$ diameter and $N_V = 20$ velocity uneven classes, spanning from 0.125 mm to 8 mm and from 0.2 m/s to 10 m/s, respectively [25]. Measurements are recorded with 1-minute integration time.

As an example, Figure 4 depicts a 1-minute spectrum collected during a rain event (April 4, 2015, 17:07 UTC): within this specific time interval, the internal software of the LPM estimates a rain rate of 34.91 mm/h. Rain rate data are available for 9 full years (2014-2022).

C. VERTICAL ATMOSPHERIC PROFILES: THE ERA5 DATASET

Another key input to the E-SST is the wind intensity v associated with the 700-mbar isobar height [18]: according to [26], v is well correlated with the precipitation translation

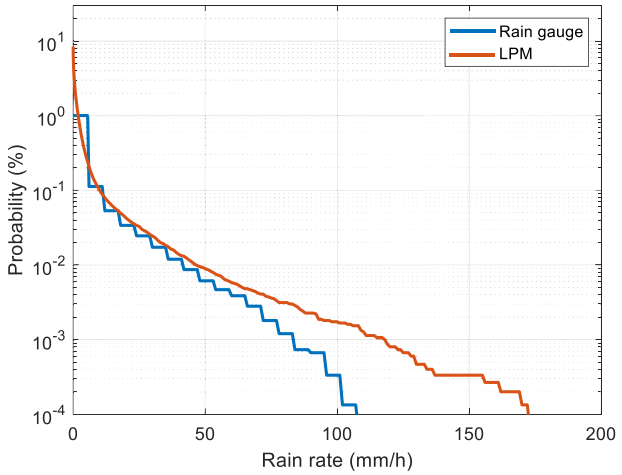

FIGURE 5. CCDF of the rain rate collected by the rain gauge (blue curve) and the LPM (red curve).

velocity. In this work, the wind data are retrieved from the European Center for Medium-range Weather Forecast (ECMWF), specifically from the ERA5 database. The main advantages of such a re-analysis database are its accuracy and quite fine resolution: the data are gathered on a regular latitude-longitude 0.25° × 0.25° grid, while the temporal resolution is 1 hour.

D. DSD FILTERING PROCESS

According to (2), accurate estimations of γ_R come with reliable values of R. A statistical comparison performed in [27] revealed that the Thies Clima disdrometer generally measures larger rainfall amounts than reference rain gauges, and it has the tendency to yield higher intensity peaks in the presence of relatively high rain rates.

The same conclusion was drawn in this contribution by comparing the Complementary Cumulative Distribution Function (CCDF) of the rain rate, as concurrently measured by the LPM (direct output of the Thies Clima processing software) and the collocated tipping rain gauge (0.1 mm accumulation tip). Though the rain gauge has a coarser quantization step (6 mm/h), the results for the full 2015-2018 period depicted in Figure 5 (i.e., when both sensors are concurrently available) clearly indicate that the two curves start deviating significantly for rain rates exceeding 60 mm/h. The LPM curve is built from the values directly estimated by the instrument software.

The rationale behind the overestimation of the LPM can be attributed to the detection and classification of falling droplets procedures performed by the disdrometer. Indeed, several mechanisms might lead to inaccuracies:

1) wind-induced horizontal drift of raindrops stimulates raindrop breakup and coalescence [28], which alter the actual DSD;
2) multiple drops simultaneously crossing the laser beam may be detected as a single larger drop [29];
3) particles hitting the rim of the light beam could be interpreted as too small;
4) drops with higher-than-expected fall velocities, typically referred to as super-terminal drops, are produced by the breakup of a large drop while they keep moving with the speed of the parent drop [30].

It is evident from the list above that the data measured by the disdrometer should be processed to compensate for those errors, as also pointed out in [31]. To this aim, the concurrent measurements collected by the collocated rain gauge (Young 52203 model, with 0.1 mm/tip resolution) can be used as reference: indeed, though also affected by measurement errors (for the Young 52203 model, the accuracy is 2% up to 25 mm/h and 3% up to 50 mm/h), rain gauges are typically considered as less sophisticated but more accurate and reliable rain sensors.

The filtering process proposed in this work aims at removing any anomalous particle from the spectra, such that the remaining ones can provide more accurate information on the DSD, leading to more reliable rain rate estimates. To this aim, the filter operates on the measured 1-minute spectrum as input. It subsequently discards particles within the ij-th bin of the aforementioned spectrum whose velocity v_j falls outside the interval I defined as

$$I = [V_{th}(D_i)(1+\alpha),\ V_{th}(D_i)(1+\beta)] \tag{8}$$

where $\alpha < 0$ and $\beta > 0$ are the filter parameters, and $V_{th}(D_i)$ is the theoretical rain drop terminal velocity with diameter D_i, drawn from the Gunn and Kinzer model [32]:

$$V_{th}(D) = 9.65 - 10.3\exp(-0.6D)\ \text{(m/s)}. \tag{9}$$

As an illustrative example, employing a filter with (α, β) set to $(-0.3, 2)$ results in the elimination of particles whose measured velocity is not included in the interval between 0.7 and 3 times the expected terminal velocity. Upon the removal of erroneous particles, the DSD can be calculated as follows [33]:

$$N(D_i) = \sum_{j=1}^{N_V} \frac{n(D_i, v_j)}{S\ V_{th}(D_i)\ T\ \Delta D_i} (\text{mm}^{-1}\text{m}^{-3}) \tag{10}$$

where $n(D_i, v_j)$ is the number of particles falling in the diameter class D_i (mm) and speed class v_j (m/s), ΔD_i (mm) represents the width of each drop-size class, $S = 4560$ (mm^2) is the LPM disdrometer sampling area, $T = 60$ (s) is the instrument integration time, $V_{th}(D_i)$ (m/s) is the terminal velocity for water drops according to the Gunn and Kinzer model, and N_V is the number of velocity classes.

The rainfall rate observed by the disdrometer is calculated from the filtered spectra by integrating the contribution of all the drops [34], as follows:

$$R = \frac{\pi}{6} \sum_{i=1}^{N_D} D_i^3 N(D_i)\ V_{th}(D_i) \Delta D_i\ \text{mm/h} \tag{11}$$

where N_D is the number of diameter classes.

The inclusion in (8) of both parameters α and β grants the filter a double degree of freedom, wherein the accuracy

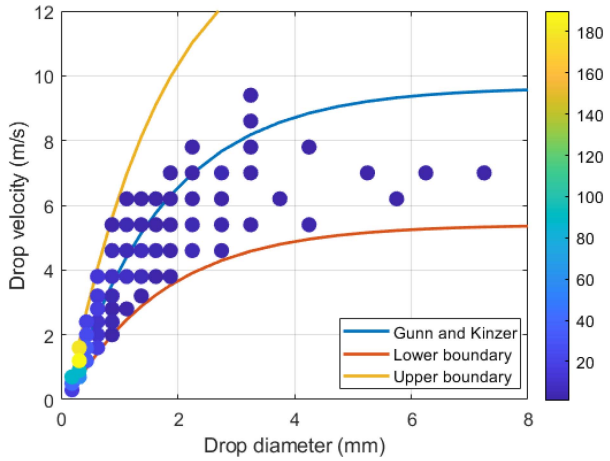

FIGURE 6. Impact of the filtering procedure on the 1-minute spectrum collected by the LPM during a rain event occurred on April 4, 2015, 17:07 UTC (see Figure 4). Resulting filtered rain rate of 19.32 mm/h. Lower boundary: $V_{th}(D_i)(1+\alpha_{opt})$; upper boundary: $V_{th}(D_i)(1+\beta_{opt})$.

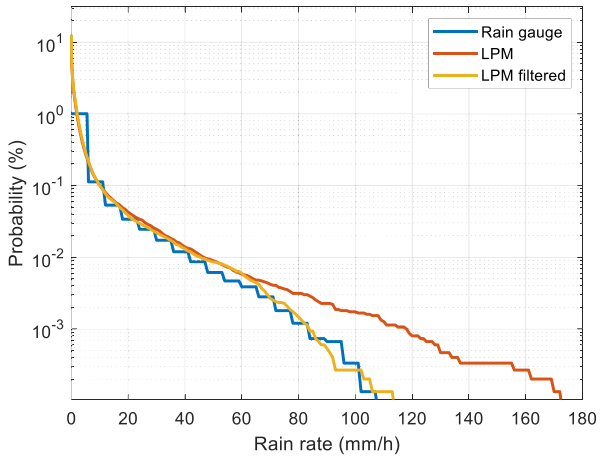

FIGURE 7. CCDF of the rain rate measured by the rain gauge (2015-2018), estimated by the internal software of the LPM (red curve) and obtained from the filtered spectra (yellow curve).

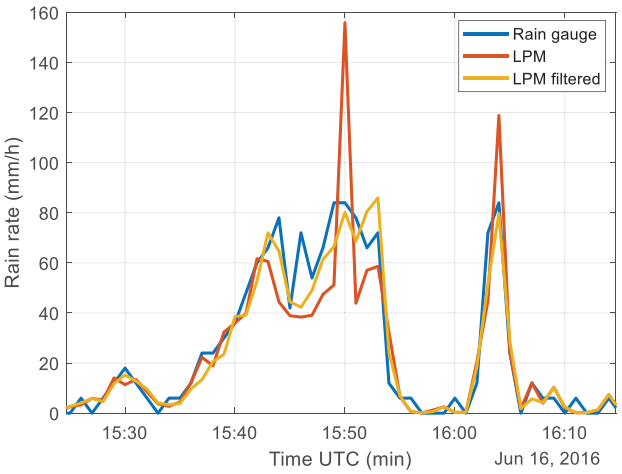

FIGURE 8. Filtering procedure applied to the convective rain event on June 16, 2016.

of the latter is contingent upon their independent selection: in this sense, a statistical comparison with the rain gauge (specifically, with the CCDF of the rain rate) permits to select the optimal pair (α_{opt}, β_{opt}). More in detail, the optimal parameters are determined by evaluating the root-mean-square (rms) value of the relative error figure ϵ_r (p, α, β) for all the possible pairs (α, β) within the range $\alpha = \{-0.8{:}0.02{:}0.3\}$ and $\beta = \{0.3{:}0.02{:}2\}$. The relative error figure ϵ_r (p, α, β) is defined as

$$\epsilon_r(p,\ \alpha, \beta) = 100\frac{R_{DSD(p,\alpha,\beta)} - R_{RG(p)}}{R_{RG}(p, \alpha,\ \beta)} \tag{12}$$

where $R_{RG}(p)$ and $R_{DSD}(p,\alpha,\beta)$ are the rain rates measured by the rain gauge and the disdrometer (the latter filtered using the specific parameters α and β), respectively, both corresponding to the same exceedance probability level $10^{-4}\% \leq p \leq 10\%$, extracted from the respective CCDFs. As a result, $\alpha_{opt} = -0.44$ and $\beta_{opt} = 0.58$ are the values minimizing the RMS (Root Mean Square) of (12).

The impact of the filtering procedure on the particle spectra can be clearly observed in Figure 6, which shows the filtered version of the spectrum depicted in Figure 4.

The effectiveness of the filter, fed with its optimal parameters, can be even more appreciated both from a statistical (see Figure 7 comparing the rain rate CCDFs) and from a time series (see Figure 8 comparing the rain rate for a sample convective event) point of view. As described in Section III-E, such a filtering approach is used to process the input rain data of the E-SST.

E. ENHANCED SYNTHETIC STORM TECHNIQUE (E-SST)

Proposed in [35] and [36], the SST is a simple yet effective approach to generate realistic time series of the rain attenuation affecting an electromagnetic wave link from the sole knowledge of the rain rate data collected at one end of the link itself. As depicted in Figure 9, by virtue of the frozen storm hypothesis and assuming a given precipitation translation speed v [37], the time t can be simply converted into distance $d = vt$.

According to the E-SST [18], the rain attenuation affecting a terrestrial link at time t_n is calculated as:

$$A_{E-SST}(t_n) = \int_{d_n}^{d_n+L} kR_S(l)^{\alpha} dl \text{ (dB)} \tag{13}$$

where R_S is the rain rate in the spatial domain, k and α are the power-law coefficients turning the rain rate into specific rain attenuation (dB/km), in this work extracted from the Recommendation ITU-R P.838-3 [19].

While in SST v is calculated as the local mean yearly wind speed [35], [36], in E-SST [18], v represents a sort of "instantaneous" value, as it is drawn from the ERA5 time series. As such data are available with 1-hour integration time, v is oversampled to 1 minute by linear interpolation [18]: as proven in [18], compared to the use of the local mean yearly wind speed value, the use of time series of v as input to the E-SST yields a higher prediction

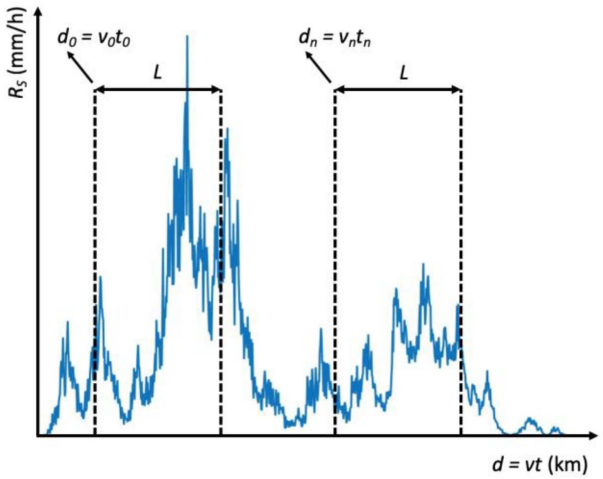

FIGURE 9. Reference outline for the application of the E-SST: identification of the rain rate values for the calculation of the rain attenuation *A* at two generic time instants, namely t_0 and t_n.

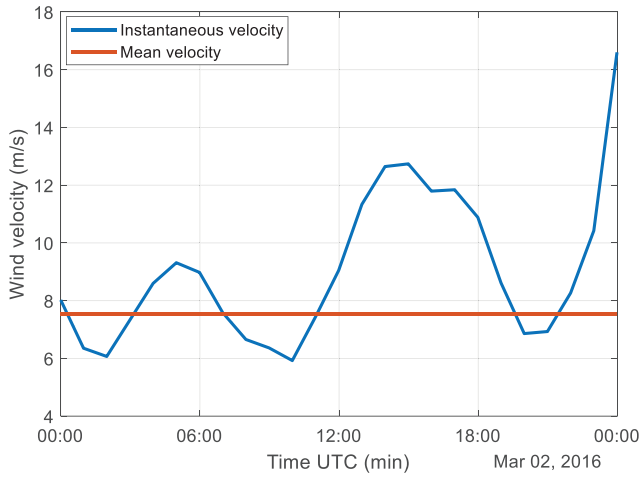

FIGURE 10. Time series of the wind velocity *v* associated with the 700-mbar isobar height, on March 2, 2016: "instantaneous" versus yearly average value.

accuracy as it allows capturing the variation of the rain event translation velocity. Figure 10 shows the pronounced temporal variability of v for a sample day, compared to its mean yearly average value $\bar{v} = 7.53$ m/s.

In this work, the E-SST was applied to estimate the rain attenuation affecting the two E-band and D-band 325-m links introduced in Section III-B (2018-2022 period). Input to the E-SST are the filtered 1-minute integrated rain rate time series collected by the LPM collocated at one end of the links. Specifically, equation (13) is discretized as follows:

$$A_{E-SST}(t_n) = \int_{d_n}^{d_n+L} kR_S(l)^\alpha dl = \sum_{i=1}^{N} k \left(R_{s,i}\right)^\alpha \Delta L \text{ (dB)} \tag{14}$$

where $R_{s,i}$ is the i-th sample of the rain rate interpolated in the spatial domain, $\Delta L = 5$ m is the sampling interval and $N = \frac{L}{\Delta L} = 65$ is the number of samples necessary to cover the entire length of the link.

TABLE 2. Average (E) and root mean square (RMS) values of the absolute error figure ε for the CCDFs reported in Figure 11 and Figure 12.

	E (dB)	RMS (dB)
E band	-0.1	0.53
D band	-0.14	0.64

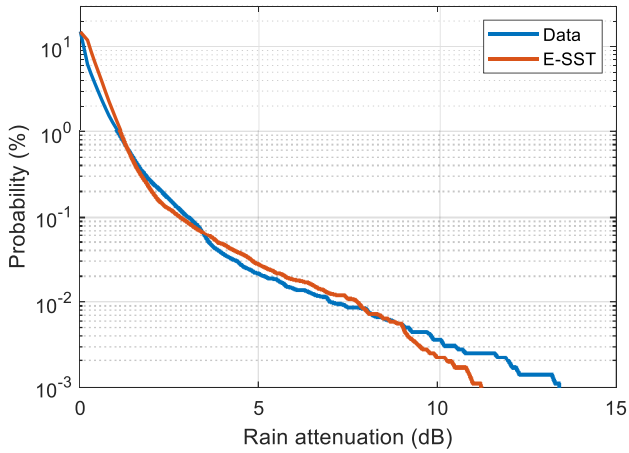

FIGURE 11. Rain attenuation at E band ($f = 83$ GHz), as estimated using the E-SST (red solid line) and as measured by the link (blue solid line).

Figure 11 and Figure 12 compare the CCDFs of the rain attenuation affecting the E-band link and the D-band one, respectively, as estimated using the E-SST and as measured by the links. Indeed, such a comparison is meaningful in the light of the accurate data processing applied to the experimental received power (see Section III-A) to remove the unwanted additional attenuation not due precipitation, but linked to system-induced effects, including the wet antenna attenuation. Results indicate a good agreement between the curves, which can be quantified by using the absolute error (dB) $\varepsilon(P) = A_{EST}(p) - A_{MEAS}(p)$. $A_{EST}(p)$ and $A_{MEAS}(p)$ represent the attenuation values (dB) extracted from the model (red line) and data (blue line) curves, respectively, both correspondent to same exceedance percentage level $10^{-3}\% < p < 10\%$. Table 2 lists the average (E) and RMS values of ε. Results definitely highlight the accuracy of the E-SST for the scenario considered in this work and corroborates its use for the calculation of PRF as shown in Section III-F.

F. PATH REDUCTION FACTOR CALCULATION: TEMPORAL APPROACH

The good prediction results shown in Section III-E for the E-SST encourage its use to calculate the PRF. To this aim though, it is better to use a larger DSD database, spanning from 2014 to 2022, in order to increase the reliability and statistical significance of the results.

Starting from the application of the E-SST, the PRF can be easily derived by inverting (3), where A is obtained by the application of (14):

$$PRF(t) = \frac{A_{E-SST}(t)}{k\ R(t)^\alpha\ L} \tag{15}$$

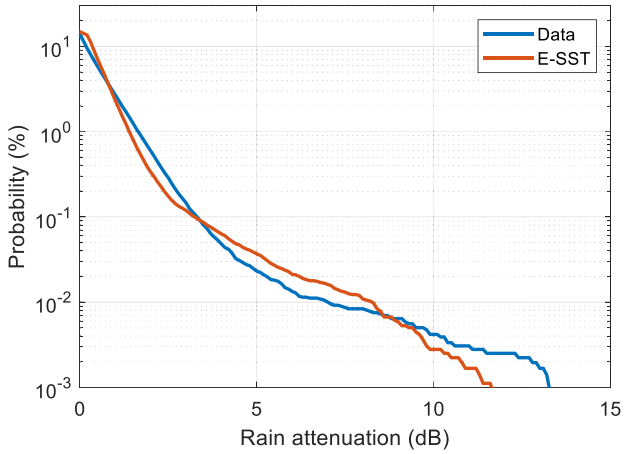

FIGURE 12. Rain attenuation at D band ($f = 156$ GHz), as estimated using the E-SST (red solid line) and as measured by the link (blue solid line).

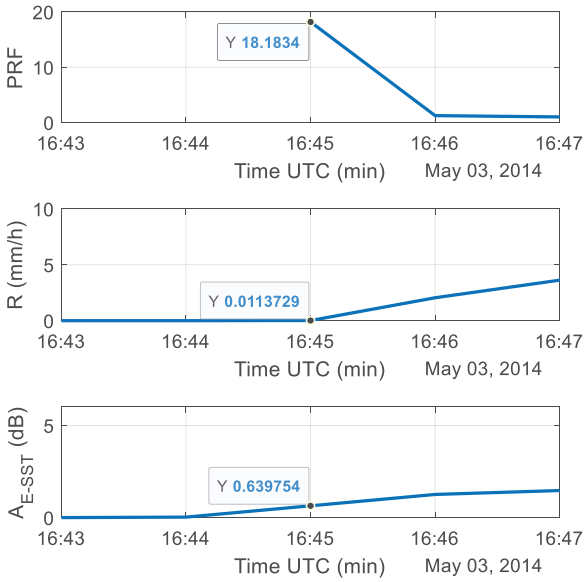

FIGURE 13. Rain attenuation estimated by the E-SST (bottom), time series of the measured rain rate (center) and the resulting PRF (top) for a rain event occurred on May 3, 2014 ($L = 400$ m, $f = 150$ GHz).

Figure 13 illustrates the concurrent temporal evolution of A_{E-SST}, of the filtered rain rate and of PRF for a rain event occurred on May 3, 2014 ($L = 400$ m and $f = 150$ GHz). Results indicate that PRF largely exceeds 1 (reaching a peak of approximately 18), which might briefly occur at the beginning of a rain event: while A_{E-SST} can be quite high due to the presence of intense precipitation along the link, the R value at the beginning of the link is very low. According to (15), these conditions yield high values of the PRF.

On the contrary, PRF values tend to be more frequently around 1 or lower than 1: this is the case reported in Figure 14, which shows the results for another event (August 24, 2018), but for instants when the rain cell is likely crossing the link.

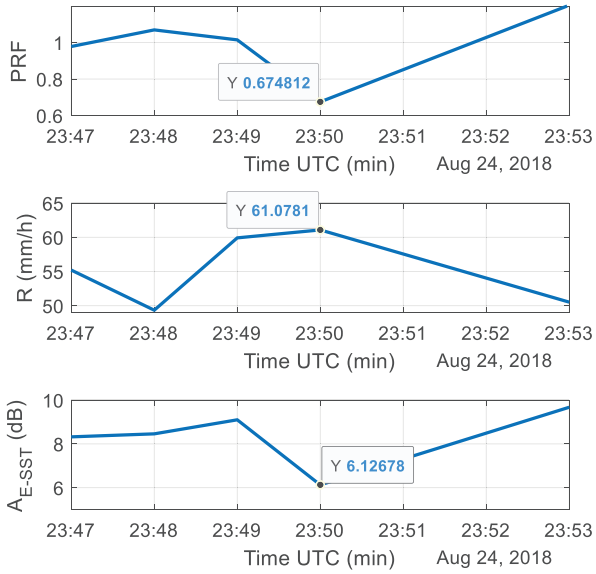

FIGURE 14. Rain attenuation estimated through the E-SST (bottom), time series of the measured rain rate (center) and the resulting PRF (top) for a rain event occurred on August 24, 2018 ($L = 400$ m, $f = 150$ GHz).

The examples shown in Figure 13 and Figure 14 clearly indicate that PRF can assume values lower or larger than 1, but they are not sufficient to draw any more general conclusion. To this aim, Figure 15 shows the R/PRF scatter plot: especially at low rain intensity values, PRF shows a significant variability, with a peak to peak variation from 0.07 to 9.6. For ease of visualization, the y-axis limit were set between 0 and 10, but some PRF values exceed the latter upper limit, as also indicated in Figure 13: however, the number of PRF values higher than 10 is quite limited, as it amounts to approximatively 0.5% of the whole dataset, for the specific scenario ($f = 150$ GHz, $L = 400$ m). For the sake of completeness, the number of PRF values exceeding 1 is roughly 8%.

The red line in Figure 15 represents the average value of PRF as a function of R, PRF_{AV}, calculated by using rain rate classes with different dimension (whose central values range from 0.4 to 166 mm/h) to include approximately the same number of points in each class, i.e., homogenize the statistical significance of the results.

Figure 16 allows a better investigation of the trend of PRF_{AV} as a function of the rain rate: its value slightly exceeds 1 for low rain rates and it decreases with the increase in R. These results reflect the fact that, the higher is the rain rate, the smaller are rain cells, i.e., the rain rate along the path is less and less homogeneous. Also, these results are in accordance with the analytical trend for PRF_{AV} proposed by some models (e.g., [10], [11], [12]), but in contrast with what is indicated by other models, namely [16] and [21]. A further conclusion can be drawn from Figure 16: there is a marginal dependence of PRF_{AV} on the operational frequency.

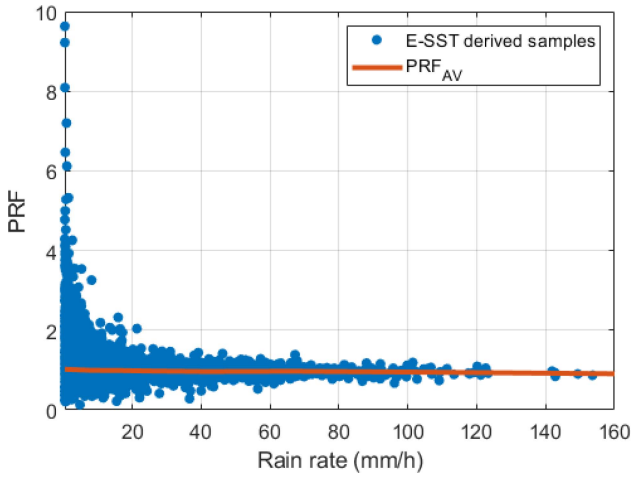

FIGURE 15. Scatter plot between PRF and R (blue points) and trend of the average PRF value (red curve) as a function of R. Dataset ranging from 2014 to 2022, $L = 400$ m, $f = 150$ GHz.

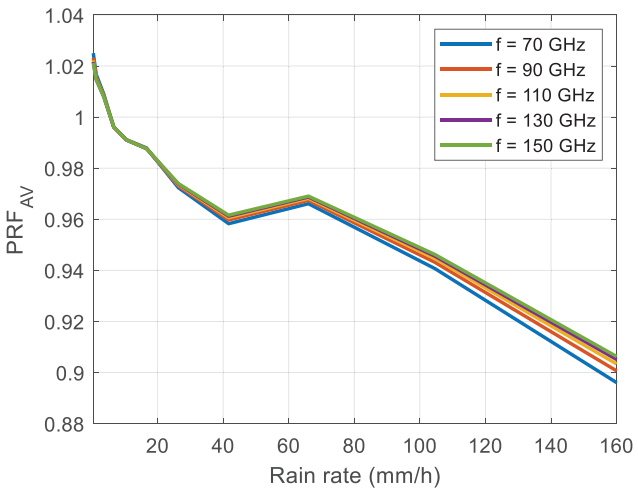

FIGURE 16. PRF_{AV} as a function of R, for different operational frequencies ($L = 400$ m).

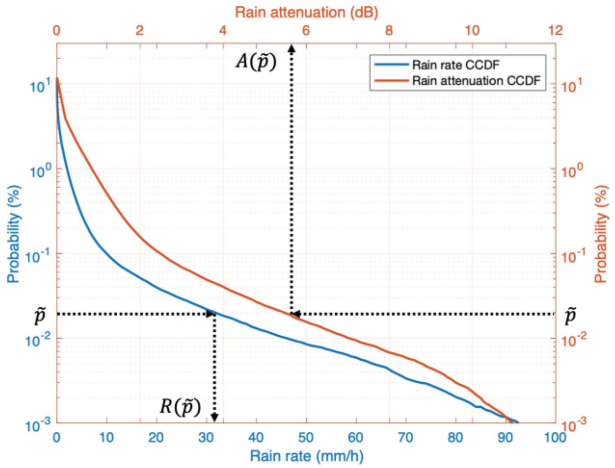

FIGURE 17. Extraction of the rain attenuation and of the rainfall rate from their respective CCDF for the calculation of PRF: values exceeded for $\tilde{p}$% of the yearly time. Dataset ranging from 2014 to 2022, $L = 400$ m, $f = 90$ GHz.

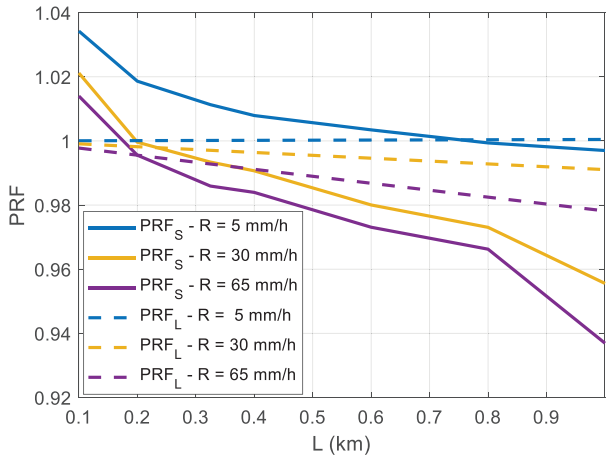

FIGURE 18. PRF_S and PRF_L as a function of the path length, plotted for different rainfall rates. Dataset ranging from 2014 to 2022, $f = 90$ GHz.

For this reason, and to more easily interpret the results, the frequency is fixed to 90 GHz for the reminder of the results shown in this contribution.

G. PATH REDUCTION FACTOR CALCULATION: STATISTICAL APPROACH

The time series analysis carried out in Section III-F highlights that PRF values can actually exceed 1, but also that PRF_{AV} has an upper limit only slightly exceeding such value. However, PRF_{AV} does not actually reflect the typical path reduction factor included in all the models discussed in this contribution: indeed, such prediction methods all have a statistical nature, i.e., the aim is the prediction of the rain attenuation CCDF using as input the CCDF of the rain rate. As a consequence, PRF is also statistical by virtue of its dependence on the rain rate exceeded with probability p. For this reason, in this Section, PRF is derived directly from the CCDFs of the rainfall rate and of the rain attenuation, i.e., through the same process typically employed in devising several models present in literature such as [10], [11], [13]. Accordingly, equation (15) becomes:

$$PRF_S(p) = \frac{A_{E-SST}(p)}{k\ R(p)^{\alpha}\ L} \tag{16}$$

where $A_{E-SST}(p)$ and $R(p)$ are the attenuation and the rainfall rate, respectively, both exceeded for p% of the yearly time (see Figure 17, relative to the case $f = 90$ GHz, $L = 400$ m).

Figure 18 depicts the trend of PRF_S derived from (16) as a function of the rain rate and of the path length ($f = 90$ GHz). While these results confirm those in Figure 16 (same trend of PRF_{AV} and PRF_S with R), they also highlight a moderate dependence of PRF_S on L. Indeed, the decrease in PRF_S with the increase in L can be explained by the fact that, the longer the link, the higher the probability to have different rain rates covering the path. For the sake of comparison, Figure 18 also includes PRF_L for the same frequency and rain rates (dashed lines), i.e., the path reduction factor of the Lin model (see Figure 1 and equation (7)): the trend of

PRF_L is in line with the one of PRF_S, though the dependence of the former on both R and L is less marked.

The approach presented in this contribution to calculate the path reduction factor presents the obvious drawback that it relies on a model: as such, one might argue that the results are of limited reliability. However, the E-SST model has proven to yield accurate results (as shown in Section III-E in this contribution, and in [18] as well) and, in addition, the results in Figure 18 appear to confirm the expected trend of PRF as a function of the rain rate and of the path length, as predicted by some models in the literature. In addition, the clear advantage of using the above-mentioned approach is the chance to avoid including in the calculation of PRF through (3) any unwanted additional attenuation that is not due to precipitation but is more linked to system-induced effects. For example: variations in the antenna gain due to partial depointing, wet antenna issues (either due to a wet film of water covering the antenna and/or to absorption of humidity), reduction in the transmit power, etc. All these effects typically contribute to increasing the attenuation along the path, which can be modeled by adding the term A_{ADD} to the rain attenuation samples obtained from E-SST:

$$A_{TOT}(t) = A_{E-SST}(t) + A_{ADD}(t) \ \text{(dB)} \tag{17}$$

A similar modeling approach is proposed in [38], which considers the effect of additional contributions to the path attenuation on measurements, where A_{ADD} is ascribed only to the wet antenna effect. Indeed, also the work in [38] proposes a rain attenuation statistics model that includes a path reduction factor limited to 1. In this work, A_{ADD} is defined as the combination of a fixed term, A_F, and of a time variant one, $A_{WA}(t)$. The former is introduced to model contributions with a limited variation in time (e.g., gas attenuation or changes in the antenna gain due to partial depointing); the latter represents the additional wet antenna attenuation, in this work modeled according to [39], where A_{WA} is estimated by spraying an antenna reflector with water. Specifically, the data from [39] used in this work are reported in Figure 19, which shows A_{WA} as a function of the rain intensity R.

The red curve in Figure 19 has the following expression:

$$A_{WA}(t) = 6.966\left(1 - 0.8497e^{-0.01681R}\right)\text{(dB)} \tag{18}$$

where the coefficients are determined by fitting the curve to the data points. The analytical model for A_{WA} is inspired by the one proposed in [15] and [40], where the same expression is used but as a function of the total measured attenuation. In this work, the dependence of A_{WA} on R in (18) is introduced to seamlessly integrate such a model with the application of E-SST: indeed, rain rate time series are the only inputs needed to calculate A_{TOT} according to (17). As a final note, it is worth underlining that, though the data in Figure 19 were obtained at Ka band and A_{WA} is expected to depend on the frequency, such data are anyway used in this work: in fact, the objective is to show how PRF is affected by

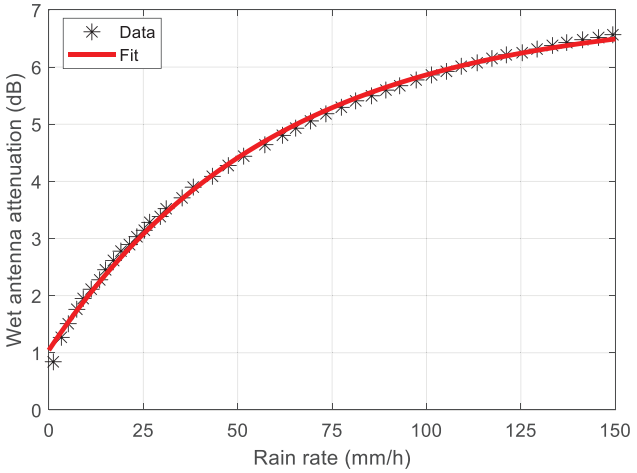

FIGURE 19. Wet antenna attenuation data extracted from [39] and associated fitting curve.

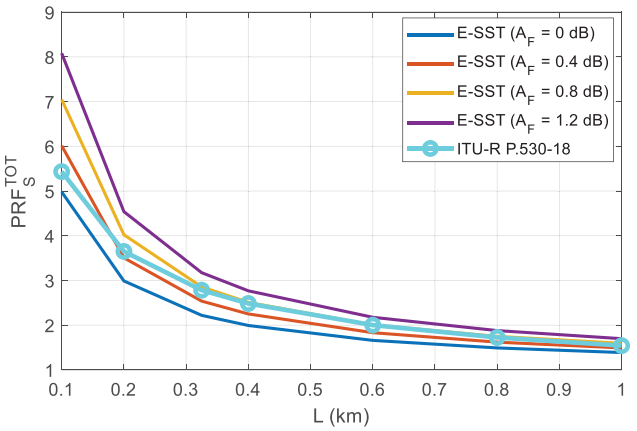

FIGURE 20. PRF_S^{TOT} as a function of the link length including the additional attenuation A_{ADD} in (17), for $R = 5$ mm/h (stratiform event) and $f = 90$ GHz. Also included is the trend of the path reduction factor as per Recommendation ITU-R P.530-18. Dataset ranging from 2014 to 2022.

additional attenuation contributions due to system-induced effects, including the wet antenna one. No similar data were found in the literature for higher frequencies.

Figure 20 and Figure 21 show the same results as in Figure 18, but obtained as:

$$PRF_S^{TOT}(p) = \frac{A_{TOT}(p)}{k\ R(p)^{\alpha}\ L} \tag{19}$$

Specifically, Figure 20 makes reference to a fixed rain rate of 5 mm/h (stratiform event) and different values of A_F: as the additional attenuation increases, so does PRF_S^{TOT}, even more so as the path length decreases. This can be explained by the fact that, while the rain attenuation obviously depends on L, A_{ADD} does not, being more bound to system features, to the wet antenna contribution and to propagation effects almost constant along the path, such as gas attenuation. As a result, the proportional weight of A_{ADD} increases gradually for shorter links, which translates in an enhanced PRF_S^{TOT} value. Figure 20 also plots the trend of the path reduction factor as predicted by the model included in recommendation

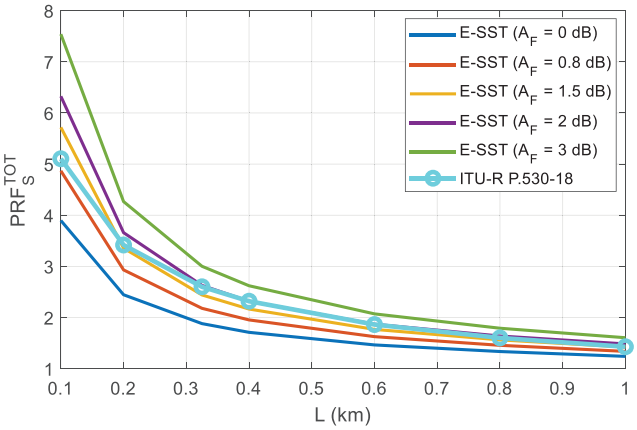

FIGURE 21. PRF_S^{TOT} as a function of the link length including the additional attenuation A_{ADD} in (17), for $R = 15$ mm/h (convective event) and $f = 90$ GHz. Also included is the trend of the path reduction factor as per recommendation ITU-R P.530-18. Dataset ranging from 2014 to 2022.

ITU-R P.530-18, PRF_{ITU} (see (5)), for the same R and f values: such trend lies between the two curves associated to $A_F = 0.4$ dB and 0.8 dB.

Figure 21 depicts the same results as in Figure 20, but for a convective rain intensity ($R = 15$ mm/h) [41]: in this case, the trend of PRF_{ITU} lies among the curves associated to $A_F = 0.8$ dB, $A_F = 1.5$ dB and $A_F = 2$ dB.

Though equation (17) offers quite a simplified approach to model additional attenuations contributions due to system-induced effects, it appears to provide a possible explanation as to why PRF_{ITU} is characterized by such a steep increase as L reduces: though this remains an open question, the attenuation measurements included in the DBSG3 database and used to derive PRF_{ITU} might not actually be representative only of the effects induced by precipitation [38].

Moreover, in some cases, additional factors might further contribute to an increased value of PRF as derived from measurements. For example, some data included in the DBSG3 database were extracted from [42], in which the authors describe a propagation experiment focused on a 0.5-km terrestrial link operating at 37, 57, 97 and 137 GHz. Three rain gauges were installed along the path to monitor the precipitation during the experimental campaign. Samples results shown in [42] (see for example Figure 7 reporting the concurrent trend of the rain intensity and of the rain attenuation measured by the links) refer to the "path-mean rainfall rate". It is evident that averaging the rain rate along a path of 0.5 km will yield lower values than those measured by a single rain gauge, even more if the event is convective, i.e., characterized by a strong spatial variability. In turn, making reference to (15), (16) and/or (19), this will produce higher values of PRF. High derived PRF values might also come from the 'total attenuation' (T) measurements included in the database: as opposed to 'excess attenuation' (E) measurements, such data also include the effects of gases, other than of rain. In approximately 62% of the entries in the DBSG3 database, no E/T information is actually provided, while for the remaining portion of the dataset, 2 entries specify that the data actually refer to total attenuation.

IV. CONCLUSION

This contribution investigates the path reduction factor, a key element of semi-empirical rain attenuation statistics prediction models, including the one adopted by ITU-R in the Recommendation P.530-18 for terrestrial links. The main goal is to provide additional elements to the debate originating from the conflicting results in the literature (i.e., PRF capped to 1, or largely greater than 1), as the link length gradually reduces to very small values (e.g., 100 m).

The novel approach relies on the use the Enhanced Synthetic Storm Technique (E-SST) to take into account the spatial inhomogeneity of precipitation along the path, from which PRF can be calculated: to the authors' knowledge, no prior work has yet proposed such an approach to investigate PRF. Moreover, the clear advantage over the more customary process of inferring PRF from measurements lies in avoiding that the derived path reduction factor expression be affected by unwanted additional attenuation not due precipitation, typically linked to system-induced effects.

The accuracy of E-SST in estimating rain attenuation statistics was corroborated by comparing the model's outcomes with the data collected for four years by two 325-m links operating at 83 GHz and 156 GHz in Milan. Besides serving as refence to test the accuracy of E-SST (careful data processing was applied to remove system-induced effects), such measurements represent a unique long-term dataset to quantify experimentally the impact of precipitation on a short link at E and D band: indeed, to the authors' knowledge, no measurements collected for four years have been published yet, especially at D band.

Based on the excellent accuracy shown by E-SST, PRF results were afterwards derived from a large set (9 years of data) of disdrometric data, which were carefully pre-processed to increase the accuracy in estimating the rain rate. To this aim, a novel approach was proposed to derive an accurate filter on the DSD data collected by the disdrometer, using as reference a collocated rain gauge. Results, obtained for hypothetical links associated to path lengths between 0.1 km and 1 km and operational frequencies in the 70-150 GHz frequency range, indicate that PRF reduces with more intense events (i.e., larger R values) and longer link, as expected due to the increase in the spatial inhomogeneity of precipitation along the path. Most importantly, the outcomes highlight that the maximum values of PRF only slightly exceeds 1 (for shorter links and less intense rain rates), in accordance with several prediction models proposed in the literature.

These results are nonetheless in contrast with the steep increase in PRF with the decrease in L, as defined by other models (including the ITU-R one): indeed, the novel approach proposed to calculate PRF offers a possible explanation to this unexpected trend of PRF, which appears to be ascribable to additional contributions to attenuation

(other than that due to precipitation) possibly affecting rain attenuation measurements (e.g., system related effects, including wet antenna issues).

ACKNOWLEDGMENT

The authors would like to thank NASA Glenn Research Center, Cleveland, OH, USA, for making disdrometric data available.

REFERENCES

[1] C. Dehos, J. L. González, A. De Domenico, D. Kténas, and L. Dussopt, "Millimeter-wave access and backhauling: The solution to the exponential data traffic increase in 5G mobile communications systems?" *IEEE Commun. Mag.*, vol. 52, no. 9, pp. 88–95, Sep. 2014.

[2] T. S. Rappaport et al., "Millimeter wave mobile communications for 5G cellular: It will work!" *IEEE Access*, vol. 1, pp. 335–349, 2013.

[3] C. Riva, C. Capsoni, L. Luini, M. Luccini, R. Nebuloni, and A. Martellucci, "The challenge of using the W band in satellite communication," *Int. J. Satellite Commun. Netw.*, vol. 32, no. 3, pp. 187–200, 2014.

[4] R. Ghiani, L. Luini, and A. Fanti, "Investigation of the path reduction factor on terrestrial links for the development of a physically-based rain attenuation model," in *Proc. EuCAP*, Apr. 2016, pp. 1–2.

[5] C. Capsoni, F. Fedi, and A. Paraboni, "A comprehensive meteorologically oriented methodology for the prediction of wave propagation parameters in telecommunication applications beyond 10 GHz," *Radio Sci.*, vol. 22, no. 3, pp. 387–393, May/Jun. 1987.

[6] L. Luini and C. Capsoni, "MultiEXCELL: A new rain field model for propagation applications," *IEEE Trans. Antennas Propag.*, vol. 59, no. 11, pp. 4286–4300, Nov. 2011.

[7] L. Luini and C. Capsoni, "The SC EXCELL model for prediction of rain attenuation on terrestrial radio links," *Electron. Lett.*, vol. 49, no. 4, pp. 307–308, Feb. 2013.

[8] U. A. Korai, L. Luini, and R. Nebuloni, "Model for the prediction of rain attenuation affecting free space optical links," *Electronics*, vol. 7, no. 12, p. 407, Dec. 2018.

[9] M. Rashid and J. Din, "Effects of reduction factor on rain attenuation predictions over millimetre-wave links for 5G applications," *Bull. Electr. Eng. Informat.*, vol. 9, no. 5, pp. 1907–1915, Oct. 2020.

[10] A. Y. Abdulrahman, T. A. Rahman, S. K. A. Rahim, and M. R. Ul Islam, "Empirically derived path reduction factor for terrestrial microwave links operating at 15 GHz in Peninsula Malaysia," *J. Electromagn. Waves Appl.*, vol. 25, no. 1, pp. 23–37, 2011.

[11] S. Lin, "11-GHz radio: Nationwide long-term rain rate statistics and empirical calculation of 11-GHz microwave rain attenuation," *Bell Syst. Tech. J.*, vol. 56, no. 9, pp. 1581–1604, Nov. 1977.

[12] F. Moupfouma, "Electromagnetic waves attenuation due to rain: A prediction model for terrestrial or L.O.S SHF and EHF radio communication links," *J. Infrared Millim. Terahertz Waves*, vol. 30, pp. 622–632, Jun. 2009.

[13] L. A. R. Da Silva Mello, M. S. Pontes, R. M. De Souza, and N. A. Perez Garcia, "Prediction of rain attenuation in terrestrial links using full rainfall rate distribution," *Electron. Lett.*, vol. 43, no. 25, pp. 1442–1443, Dec. 2007.

[14] R. Ghiani, L. Luini, and A. Fanti, "A physically based rain attenuation model for terrestrial links," *Radio Sci.*, vol. 52, no. 8, pp. 972–980, Aug. 2017.

[15] L. Luini, G. Roveda, M. Zaffaroni, M. Costa, and C. Riva, "The impact of rain on short *E*-band radio links for 5G mobile systems: Experimental results and prediction models," *IEEE Trans. Antennas Propag.*, vol. 68, no. 4, pp. 3124–3134, Apr. 2020.

[16] A. A. H. Budalal, M. R. Islam, K. Abdullah, and T. A. Rahman, "Modification of distance factor in rain attenuation prediction for short-range millimeter-wave links," *IEEE Antennas Wireless Propag. Lett.*, vol. 19, no. 6, pp. 1027–1031, Jun. 2020.

[17] A. A. Hussein Budalal, "Millimeter-wave propagation modeling for 5G based on rain fade data in tropical climate," Kulliyyah Eng., Int. Islamic Univ. Malaysia, Selangor, Malaysia, 2022.

[18] L. Luini, A. Panzeri, and C. Riva, "Enhancement of the synthetic storm technique for the prediction of rain attenuation time series at EHF," *IEEE Trans. Antennas Propag.*, vol. 68, no. 7, pp. 5592–5601, Jul. 2020.

[19] "Specific attenuation model for rain for use in prediction methods," ITU, Geneva, Switzerland, ITU-R P. 838–3, 2005.

[20] L. Féral, H. Sauvageot, L. Castanet, J. Lemorton, F. Cornet, and K. Leconte, "Large-scale modeling of rain fields from a rain cell deterministic model," *Radio Sci.*, vol. 41, no. 2, pp. 1–21, 2006.

[21] "Propagation data and prediction methods required for the design of terrestrial line-of-sight systems," ITU, Geneva, Switzerland, ITU-R P530–18, 2021.

[22] A. M. Musthafa, L. Luini, C. Riva, S. N. Livieratos, and G. Roveda, "A long-term experimental investigation on the impact of rainfall on short 6G D-band links," *Radio Sci.*, vol. 58, no. 5, pp. 1–10, May 2023.

[23] "Attenuation by atmospheric gases and related effects," ITU, Geneva, Switzerland, Recommendation ITU-R P. 676.-13, 2022.

[24] S. K. A. Rahim, A. Y. Abdulrahman, T. A. Rahman, and M. R. Ul Islam, "Measurement of wet antenna losses on 26 GHz terrestrial microwave link in Malaysia," *Wireless Pers. Commun. Now.*, vol. 64, no. 2, pp. 225–231, 2012.

[25] "Thies clima laser precipitation monitor," document Rev. 2.5, Jul. 2011. [Online]. Available: https://www.thiesclima.com/

[26] L. Luini and N. Jeannin, "Use of weather radar data for site diversity predictions and impact of rain field advection," in *Proc. 4th Adv. Satellite Mobile Syst.*, Bologna, Italy, 2008, pp. 122–127.

[27] L. G. Lanza and E. Vuerich, "The WMO field intercomparison of rain intensity gauges," *Atmosph. Res.*, vol. 94, pp. 534–543, Dec. 2009. doi: 10.1016/j.atmosres.2009.06.012.

[28] F. Y. Testik and B. Pei, "Wind effects on the shape of raindrop size distribution," *J. Hydrometeorol.*, vol. 18, no. 5, pp. 1–19, 2017, doi: 10.1175/JHM-D-16-0211.1.

[29] M. Fehlmann, M. Rohrer, A. von Lerber, and M. Stoffel, "Rainfall amount and intensity measured by the Thies laser precipitation monitor," *Atmos. Meas. Tech.*, vol. 13, pp. 4683–4698, Jan. 2020.

[30] G. Montero-Martínez, A. B. Kostinski, R. A. Shaw, and F. García-García, "Do all raindrops fall at terminal speed?" *Geophys. Res. Lett.*, vol. 36, no. 11, pp. 1–4, 2009.

[31] J. M. Riera et al., "Characterization of rain attenuation in 80–200 GHz from experimental drop size distributions," *IEEE Trans. Antennas Propag.*, vol. 71, no. 5, pp. 4371–4379, May 2023.

[32] R. Gunn and G. D. Kinzer, "The teminal velocity of fall for water droplets in stagnant air," *J. Atmosph. Sci.*, vol. 6, no. 4, pp. 243–248, 1949.

[33] H. Y. Lam, L. Luini, J. Din, C. Capsoni, and A. D. Panagopoulos, "Investigation of rain attenuation in equatorial Kuala Lumpur," *IEEE Antennas Wireless Propag. Lett.*, vol. 11, pp. 1002–1005, 2012.

[34] J. M. Riera, A. Benarroch, P. Garcia-del-Pino, and S. Pérez-Peña, "Preprocessing and assessment of rain drop size distributions measured with a K-band Doppler radar and an optical disdrometer," *IEEE Trans. Instrum. Meas.*, vol. 70, pp. 1–8, 2021, doi: 10.1109/TIM.2020.3007909.

[35] G. Drufuca, "Rain attenuation statistics for frequencies above 10 GHz from rain gauge observations," *J. Rech. Atmos.*, vol. 1, pp. 399–411, Nov. 1974.

[36] E. Matricciani, "Physical–mathematical model of the dynamics of rain attenuation based on rain rate time series and two–layer vertical structure of precipitation," *Radio Sci.*, vol. 31, no. 2, pp. 281–295, Mar./Apr. 1996.

[37] G. I. Taylor, "The spectrum of turbulence," *Proc. Roy. Soc. London A Math. Phys. Sci.*, vol. 164, no. 919, pp. 476–490, 1938.

[38] X. Zhang et al., "Rain attenuation prediction model for terrestrial links incorporating wet antenna effects," *IET Microw. Antennas Propag.*, vol. 17, pp. 634–641, Jul. 2023.

[39] R. K. Crane, "Analysis of the effects of water on the ACTS propagation terminal antenna," *IEEE Trans. Antennas Propag.*, vol. 50, no. 7, pp. 954–965, Jul. 2002.

[40] M. M. Z. Kharadly and R. Ross, "Effect of wet antenna attenuation on propagation data statistics," *IEEE Trans. Antennas Propag.*, vol. 49, no. 8, pp. 1183–1191, Aug. 2001.

[41] C. Capsoni, L. Luini, A. Paraboni, and C. Riva, "Stratiform and convective rain discrimination deduced from local P(R)," *IEEE Trans. Antennas Propag.*, vol. 54, no. 11, pp. 3566–3569, Nov. 2006.

[42] C. J. Gibbins et al., "A 500 m experimental range for propagation studies at millimetre, infrared and optical wavelengths," *J. Inst. Electron. Radio Eng.*, vol. 57, no. 5, pp. 227–234, Sep./Oct. 1987.

FRANCESCO CAPELLETTI was born in Italy in 1997. He received the B.Sc. degree in engineering of computing systems and the M.Sc. degree in telecommunication engineering from Politecnico di Milano, Italy, in 2021 and 2023, respectively, where he is currently pursuing the Ph.D. degree in information technology with the Dipartimento di Elettronica, Informazione e Bioingegneria. His main research studies cover the propagation of electromagnetic waves in terrestrial and nonterrestrial radio systems, particularly focused on predicting the detrimental impact of the atmosphere, as well as on modeling of interference and frequency management within radio-frequency systems. He is also involved in the "Enhanced Alphasat Aldo Paraboni QV Band Test-Bed Configurations for Additional Experiments" (CALIBRATE) Project, commissioned by the European Space Agency.

CARLO RIVA (Senior Member, IEEE) received the Laurea degree in electronic engineering and the Ph.D. degree in electronic and communication engineering from the Politecnico di Milano, Milan, Italy, in 1990 and 1995, respectively. In 1999, he joined the Dipartimento di Elettronica, Informazione e Bioingegneria, Politecnico di Milano, where, since 2020, he has been a Full Professor of Electromagnetic Fields. He participated in the Olympus, Italsat, and (the running) Alphasat Aldo Paraboni (for this experiment, he has been appointed as Principal Investigator by ASI in 2012) propagation measurement campaigns, in the COST255, COST280, and COSTIC0802 international projects on propagation and telecommunications and in the Satellite Communications Network of Excellence (SatNEx). He served as an Associate Editor for IEEE TRANSACTIONS ON ANTENNAS AND PROPAGATION from 2017 to 2023 and he is the Chairman of WP 3J of ITU-R SG3 ("Propagation Fundamentals"). He is the author of about 280 papers published in international journals or international conference proceedings. His main research activities are in the field of the tropospheric effects in satellite microwave links (GEO, MEO, LEO, and Deep Space) and their statistical and physical modeling, the propagation impairment mitigation techniques, and satellite communication adaptive systems.

GIUSEPPE ROVEDA received the M.Sc. degree in electronic engineering from Politecnico di Milano, Italy, in 1992. He has got 25+ years' experience in tier-1 telecommunication companies (Italtel, Ericsson, and Huawei) dealing with mobile systems along their subsequent generations starting from GSM up to 5G and over. He is currently a Microwave System Engineer with Huawei Technologies Italy, where he is involved in propagation, interference, and coexistence studies at millimeter wave and in standardization, regulatory, and spectrum engineering areas at ITU-R, CEPT/ECC, and ETSI within different technical committees (WP5D, WP3J/K, WG SE, PT1, SE19, SE21, SE40, and ISG mWT).

LORENZO LUINI (Senior Member, IEEE) was born in Italy in 1979. He received the Laurea degree (cum laude) in telecommunication engineering and the Ph.D. degree (cum laude) in information technology from Politecnico di Milano, Italy, in 2004 and 2009, respectively, where he is currently an Associate Professor with the Dipartimento di Elettronica, Informazione e Bioingegneria. His research activities are focused on electromagnetic wave propagation through the atmosphere, both at radio and optical frequencies. He also worked as a System Engineer with the Industrial Unit, Global Navigation Satellite System Department, Thales Alenia Space Italia S.p.A. He has been involved in several European COST projects, in the European Satellite Network of Excellence (SatNEx), as well as in several projects commissioned to the research group by the European Space Agency, the USA Air Force Laboratory (AFRL), and the European Commission (H2020). He authored 240 contributions to international conferences and scientific journals. He is an Associate Editor of IEEE TRANSACTIONS ON ANTENNAS AND PROPAGATION and *International Journal on Antennas and Propagation*, a member of the Italian Society of Electromagnetism, a Board Member of the Working Group "Propagation" of European Association on Antennas and Propagation (EurAAP), and a Leader of Working Group "Propagation Data Calibration" within the AlphaSat Aldo Paraboni Propagation Experimenters (ASAPE) Group.

Open Access funding provided by 'Politecnico di Milano' within the CRUI CARE Agreement